ACS APPLIED MATERIALS & INTERFACES

Research Article

Cite This: ACS Appl. Mater. Interfaces 2018, 10, 35462−35468

www.acsami.org

# Combining Linker Design and Linker-Exchange Strategies for the Synthesis of a Stable Large-Pore Zr-Based Metal−Organic Framework

Hue T. T. Nguyen,[†,‡] Thach N. Tu,[*,‡,§] My V. Nguyen,[†,‡] Tien H. N. Lo,[†,⊥,‡] Hiroyasu Furukawa,[∥] Ngoc N. Nguyen,[†,§,‡] and My D. Nguyen[§,‡]

[‡]Center for Innovative Materials and Architectures (INOMAR)and [†]University of Science, Vietnam National University-Ho Chi Minh (VNU-HCM), Ho Chi Minh City 721337, Vietnam

[§]Nguyen Tat Thanh University, 300A Nguyen Tat Thanh Street, District 4, Ho Chi Minh City 755414, Vietnam

[∥]Department of Chemistry, University of California, Berkeley, California 94720, United States

Supporting Information

**ABSTRACT:** A Zr(IV)-based metal−organic framework (MOF), termed **reo**-MOF-1 [$Zr_6O_8(H_2O)_8(SNDC)_4$], composed of 4-sulfonaphthalene-2,6-dicarboxylate ($HSNDC^{2-}$) linkers and $Zr_6O_8(H_2O)_8(CO_2)_8$ clusters was synthesized by solvothermal synthesis. Structural analysis revealed that **reo**-MOF-1 adopts the **reo** topology highlighted with large cuboctahedral cages (23 Å). This structure is similar to that found in DUT-52 (**fcu** topology), however, **reo**-MOF-1 lacks the body-centered packing of the 12-connected $Zr_6O_4(OH)_4(CO_2)_{12}$ clusters, which is attributed to the subtle, but crucial influence in the bulkiness of functional groups on the linkers. The control experiments, where the ratio of $H_3SNDC$/naphthalene-2,6-dicarboxylate linkers was varied, also support our finding that the bulky functionalities play a key role for defect-controlled synthesis. The **reo**-MOF-$1_A$ framework was obtained by linker exchange to yield a chemically and thermally stable material despite its large pores. Remarkably, **reo**-MOF-$1_A$ exhibits permanent porosity (Brunauer−Emmett−Teller and Langmuir surface areas of 2104 and 2203 $m^2\ g^{-1}$, respectively). Owing to these remarkable structural features, **reo**-MOF-$1_A$ significantly enhances the yield in Brønsted acid-catalyzed reactions.

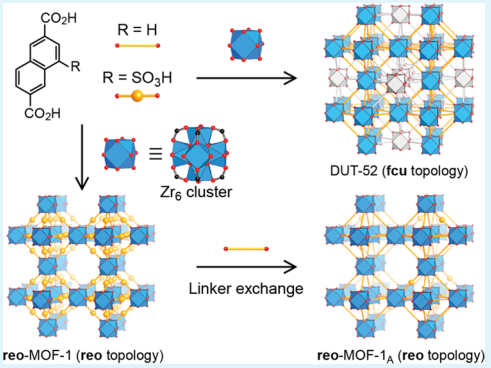


**KEYWORDS:** *MOF, defect, Brønsted acid catalyst, reo topology*

## 1. INTRODUCTION

Metal−organic frameworks (MOFs) are a new generation of porous extended materials assembled by inorganic and organic building units. Judicious selection of these building units leads to various crystalline architectures with tunable pore sizes and shapes. Internal chemical environments can also be modified by introducing functionalized building units into the framework.[1] Due to such amenability in the design and synthesis of MOF structures, significant efforts have been devoted for employing MOFs in a wide range of applications, including but not limited to gas storage/separation[2,3] proton conduction,[4−6] catalysis,[7,8] and drug delivery.[9,10] Among the tens of thousands of MOFs that have been synthesized to date, Zr-based MOFs have received considerable attention due to their remarkable chemical stability[11,12] and mechanical strength,[13,14] which are important properties for the use of MOFs in practical applications.[15] However, most Zr-based MOFs synthesized with simple organic linkers have relatively small pores,[15,16] which restricts the use of Zr-based MOFs in catalysis.

A popular technique to overcome this limitation is defect-controlled synthesis,[17−19] as the presence of random defect sites distributed throughout the framework results in hierarchical pore architectures consisting of micro- and meso-/macropores. Further, deliberate incorporation of defect sites into MOFs often leads to emerging properties that cannot be replicated in the "defect-free" MOFs, including enhanced porosity[20,21] and gas uptake properties,[22,23] proton conductivity,[24,25] and catalytic activity,[26,27] as well as the removal of toxic contaminants (e.g., organic vapors and metal ions).[28−31] Several strategies have been proposed for defect-controlled synthesis, including modulating the crystallization rate during MOF formation,[32,33] addition of modulators (typically monocarboxylic acids),[22,29,34−36] and linker thermolysis.[37−40] Specifically designed organic linkers are also utilized to introduce higher porosity in these frameworks in a controlled manner.[24,41,42] The essence of this approach is that bulky functionalities of the linker can induce the formation of inorganic clusters with a lower coordination number (e.g.,

Received: July 3, 2018
Accepted: September 18, 2018
Published: September 18, 2018






DOI: 10.1021/acsami.8b11037
ACS Appl. Mater. Interfaces 2018, 10, 35462−35468

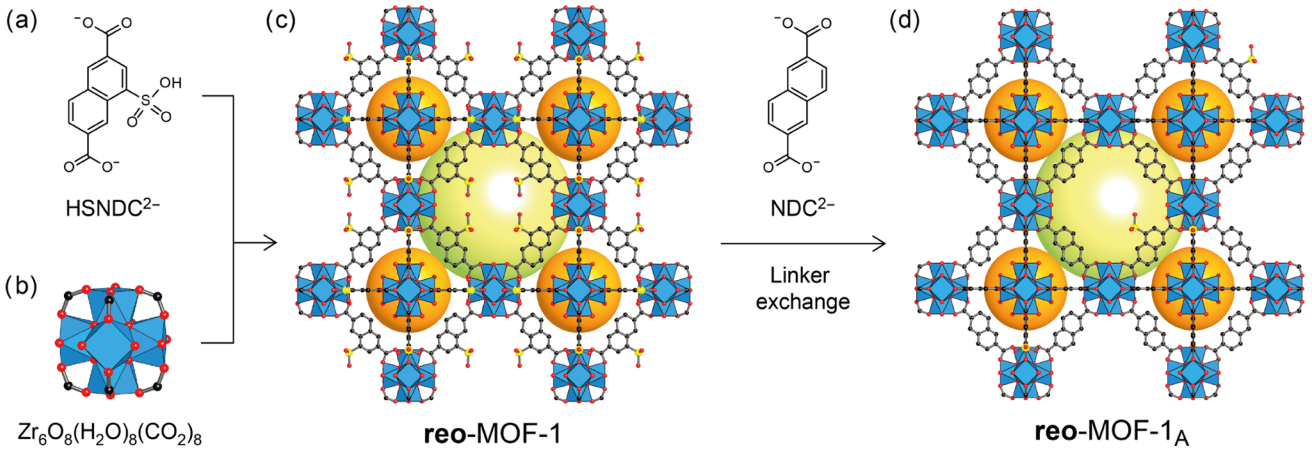


**Figure 1.** Backbone structure of **reo**-MOF-1 (c) is constructed from $Zr_6O_8(H_2O)_8(CO_2)_8$ clusters (a) and ditopic $HSNDC^{2-}$ linkers (b), whose connectivity is found to be based on the **reo** architecture. This structure is identical to the **fcu** architecture with the missing cluster defect featured with two types of cages. Linkers of **reo**-MOF-1 were further exchanged with $NDC^{2-}$ to obtain **reo**-MOF-$1_A$ (d). Atom colors: Zr, blue polyhedra; C, black; O, red; S, yellow. All hydrogen atoms are omitted for clarity.

12-coordinated $Zr_6O_4(OH)_4(CO_2)_{12}$ vs 8-coordinated $Zr_6O_8(H_2O)_8(CO_2)_8$). Consequently, the probability of generating defect sites increases as there are fewer connections between inorganic clusters.[24,41,42]

Despite the promises for designing the defect-controlled MOFs with higher surface area (SA), this strategy suffers some drawbacks: (i) reduced mechanical stability, leading to structural degradation during desolvation (for example, the presence of sulfonic acid groups in UiO-66 drives this material to collapse during activation)[41,43] and (ii) the pore window may be blocked by the dangling functional groups, preventing large guest molecules accessing the pore interior.[21]

To overcome these challenges, we propose a two-step synthesis of a Zr-based MOF that possesses a chemically and mechanically stable framework with enlarged pores by combining linker design (i.e., addition of bulky functional groups) and postsynthetic linker-exchange strategies. More specifically, this approach was implemented by assembling 4-sulfonaphthalene-2,6-dicarboxylate ($HSNDC^{2-}$) as the linker with $Zr_6O_8(H_2O)_8(CO_2)_8$ inorganic clusters. The presence of the sulfonate moieties tethered to the ditopic linkers leads to a framework with enlarged pores, termed **reo**-MOF-1. Structural analysis revealed that the topology of **reo**-MOF-1 is found to be based on the **reo** net, which is reminiscent of the **fcu** net with the missing metal cluster "defect".[44] The resulting powder sample was further treated with naphthalene-2,6-dicarboxylate ($NDC^{2-}$) to obtain the open-pore material, namely, **reo**-MOF-$1_A$. As expected, the linker-exchanged material exhibits permanent porosity (Brunauer–Emmett–Teller (BET) SA = 2104 $m^2\ g^{-1}$). Furthermore, owing to the presence of large cages (23 Å) decorated with sulfonic acid moieties (residual $HSNDC^{2-}$ after the linker exchange), **reo**-MOF-$1_A$ exhibits higher catalytic activity than that of **reo**-MOF-1, DUT-52, UiO-66, UiO-67, MOF-808, and NU-1000 for Brønsted acid catalytic reactions.[45−48]

## 2. EXPERIMENTAL SECTION

**2.1. Chemicals.** *N*,*N*-Dimethylformamide (DMF), formic acid (purity >98%), dichloromethane, and anhydrous methanol were obtained from EMD Millipore Chemicals. Zirconium oxychloride octahydrate ($ZrOCl_2{\cdot}8H_2O$, purity ≥99.5%) and naphthalene-2,6-dicarboxylic acid ($H_2NDC$, >95%) were obtained from Sigma-Aldrich. Oleum was obtained from a local commercial vendor. All starting materials and solvents were used without further purification. $H_3SNDC$ was synthesized according to the published procedure.[49]

**2.2. Synthesis of reo-MOF-1.** A mixture of $ZrOCl_2{\cdot}8H_2O$ (0.056 g, 0.17 mmol) and $H_3SNDC$ (0.048 g, 0.16 mmol) was dissolved in 8 mL of DMF. Subsequently, formic acid (2 mL) was added into the solution. The reaction mixture was heated at 120 °C in an isothermal oven for 24 h, then cooled to room temperature. The resulting crystalline powder was collected by centrifugation, washed with DMF (10 mL) and methanol (10 mL) for 3 days, respectively, during which DMF and methanol were decanted and replenished three times per day. The product was evacuated under vacuum ($10^{-3}$ Torr) at room temperature to yield the white guest-free solid (80% yield, based on $Zr^{4+}$). Elemental analysis (EA) of activated sample: calcd for $Zr_6C_{53.4}H_{77.4}O_{56.5}N_{2.2}S_4$ = $[Zr_6O_7(OH)(H_2O)_6(SNDC)_{2.2}$-$(HSNDC)_{1.8}(HCO_2)]{\cdot}2.2(C_2H_8N){\cdot}12.5(H_2O)$: C, 27.52; H, 3.32; N, 1.32, and S, 5.50%. Found: C, 27.99; H, 3.19; N, 1.49, and S, 5.13%. Fourier transform infrared (attenuated total reflectance) (FT-IR (ATR)): 1654 (s); 1605 (m); 1561 (s); 1494 (w); 1414 (s); 1354 (s); 1190 (s); 1172 (s); 1046 (s); 998 (m); 925 (m); 842 (w); 788 (s); 765 (s); 722 (w); 650 (w); and 619 (s) (Figure S9).

**2.3. Synthesis of Linker-Exchanged reo-MOF-1 (reo-MOF-$1_A$).** $H_2NDC$ (500 mg) was dissolved in 3 mL of KOH solution (4% in $H_2O$), in which 1 M HCl was added to adjust the pH of the mixture to 8. The powder material of **reo**-MOF-1 (50 mg) was added to the solution containing the linker and stirred at room temperature for 30 min. The linker-exchanged MOF powder was centrifuged and washed with water (10 mL) for 24 h, during which the water was decanted and replenished five times to remove unreacted $K_2NDC$. After washing, the MOF powder sample was immersed in an acidified MeOH/$H_2O$ (= 8:2, v/v; pH was adjusted to 1 with 1 M HCl) solution for 24 h and washed with MeOH/$H_2O$ (= 8:2, v/v) until the pH of the decanted liquor reached to 4. The recovered MOF powder was further washed with DMF (3 × 5 mL, 24 h), MeOH (5 × 5 mL, 24 h), $CH_2Cl_2$ (5 × 5 mL, 24 h), successively, and dried under dynamic vacuum ($10^{-3}$ Torr) at room temperature to yield the desolvated **reo**-MOF-$1_A$ material. EA of activated sample: calcd for $Zr_6C_{60}H_{48.92}O_{39.13}S_{0.62}$ = $[Zr_6O_7(OH)(H_2O)_6(NDC)_{4.38}$-$(HSNDC)_{0.62}]{\cdot}3.27(H_2O)$: C, 36.52; H, 2.48; N, 0; and S, 1.00%. Found: C, 36.71; H, 2.49; N, 0.07; and S, 1.54%. FT-IR (ATR): 1695 (w); 1604 (s); 1556 (s); 1493 (m); 1414 (s); 1358 (s); 1196 (s); 1142 (w); 1108 (w); 1047 (m); 999 (w); 968 (w); 921 (m); 829 (w); 784 (s); and 639 (s) (Figure S9).

## 3. RESULTS AND DISCUSSION

**3.1. Synthesis, Structural Determination, and Characterization of reo-MOF-1.** A microcrystalline powder of


DOI: 10.1021/acsami.8b11037
ACS Appl. Mater. Interfaces 2018, 10, 35462−35468

**reo**-MOF-1 was solvothermally synthesized from $H_3SNDC$ linker and $ZrOCl_2{\cdot}8H_2O$ in DMF with the presence of formic acid as a modulator (Figure 1). Powder X-ray diffraction (PXRD) pattern of the as-synthesized sample exhibits four intense diffraction peaks at $2\theta$ = 3.75, 5.29, 6.48, and 7.48°, whose profile is different from the calculated PXRD pattern of DUT-52 [$Zr_6O_4(OH)_4(NDC)_6$] (Figures 2 and S3).[45,50]

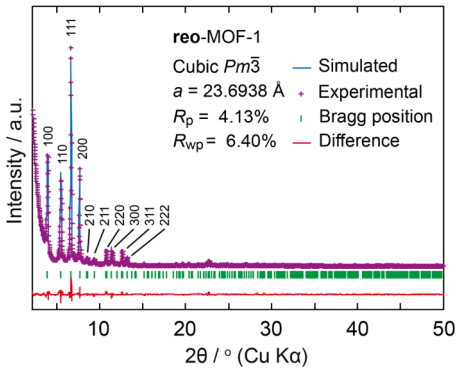


**Figure 2.** Experimental (purple) and refined (blue) PXRD patterns of as-synthesized **reo**-MOF-1 after Rietveld refinement. The difference plot (red) and Bragg positions (green) are also provided. Full range Rietveld refinement data ($2\theta$ = 2−80°) are shown in the Supporting Information (Section S4).

To investigate whether the **reo**-MOF-1 structure is formed by the introduction of defect sites into the DUT-52 framework (face-centered cubic, $Fm\bar{3}m$, **fcu** topology), MOF samples containing two linkers (i.e., $HSNDC^{2-}$ and $NDC^{2-}$) with variable ratios were prepared (Section S3). The PXRD patterns of these materials revealed that the relative intensity of two low angle peaks ($2\theta$ = 3.75 and 5.29°) increases with a larger amount of $H_3SNDC$ added to the reaction mixture, whereas the unit cell length of a series of mixed-linker MOFs is nearly identical to that found in DUT-52 (Figures S4 and S5). Furthermore, given the position of two extra diffraction peaks at low angle, the Bravais lattice of defect containing MOFs must be in the primitive cubic system ($P23$, $Pm\bar{3}$, $P432$, $P\bar{4}3m$, or $Pm\bar{3}m$). This finding indicates that the introduction of the defect sites (i.e., missing clusters) lowers the symmetry of mixed-linker MOF samples.

To elucidate the atomistic connectivity of **reo**-MOF-1, powder pattern indexing, followed by profile fitting, was performed using Materials Studio Version 7.0 software. Analysis of the diffraction data from the as-synthesized **reo**-MOF-1 material indicates that the framework crystallizes in the cubic space group $Pm\bar{3}$ (No. 200), with a unit cell length of 23.6938 Å. This implies that Zr clusters in **reo**-MOF-1 are bridged by $SNDC^{3-}$/$HSNDC^{2-}$ linkers[51] as observed in DUT-52, whereas 12-connected $Zr_6O_4(OH)_4(CO_2)_{12}$ clusters at the body-centered position in DUT-52 are not present in the **reo**-MOF-1 framework since we observe reflections that would be forbidden in a body-centered unit cell. With this modeled structure, the full range Rietveld refinement was performed to optimize the atom position in the lattice, with the structure being successfully refined with low $R$-values ($2\theta$ = 2−80°, $R_p$ = 4.13%, and $R_{wp}$ = 6.4%, Figures 2 and S7, Section S4).

The refined structure clearly reveals that **reo**-MOF-1 consists of eight-connected $Zr_6O_8(H_2O)_8(CO_2)_8$ clusters, which are linked by $SNDC^{3-}$/$HSNDC^{2-}$ linkers (Figure 1a,b) to realize the **reo** net (Figure S8) with eight corner-shared octahedral cages (9 Å) around the central cuboctahedral cage (23 Å) (Figure S8). These two types of cage are cross-linked through a triangular window with an aperture diameter of approximately 5 Å. It should be noted that although several Zr-based MOFs with the **reo** net have been reported (DUT-51, DUT-67, and UiO-66 containing missing cluster defects),[34,52,53] these MOFs are synthesized by making use of either bent linkers or modulators. In contrast, the generation of defects in **reo**-MOF-1 is attributed to the subtle difference in the bulkiness of functionalities (i.e., DUT-52 vs **reo**-MOF-1, Figure S8). Considering the coordination number of Zr-based clusters that can be readily manipulated by introducing bulky functionalities,[24,41,42] this approach is valuable as a means of manipulating framework connectivity, especially, for MOFs composed of high coordination number inorganic units.[24,41,42]

To investigate the architectural stability of **reo**-MOF-1, the as-synthesized material was washed with DMF and MeOH, followed by evacuation under dynamic vacuum at room temperature. FT-IR spectroscopy of desolvated **reo**-MOF-1 demonstrates that the atomistic connectivity of **reo**-MOF-1 is unchanged, as observed by the presence of coordinated carboxylate with the characteristic sharp signals indicative of carboxylate groups (C═O), appearing at 1649 and 1600 $cm^{-1}$ (multipeaks are caused by the asymmetry of the $SNDC^{3-}$ linker). The presence of sulfonate moieties was also confirmed by the broad peak at 1180 $cm^{-1}$ (Figures 3a and S9). However, PXRD analysis indicates that the crystallinity of the desolvated materials is lower than that of as-synthesized materials, which is indicative of the loss of long range periodicity in the materials (Figure 3b). Considering that a similar trend was observed in MOFs possessing sulfonate functionalities,[41,43] the removal of methanol from the cage without sacrificing the crystallinity may be hampered by the strong interaction between the sulfonate groups and methanol. This is also in line with the $N_2$ adsorption analysis; the BET surface area of the desolvated material was estimated to be 34 $m^2\ g^{-1}$, which is significantly lower than the theoretically predicted value (Materials Studio Version 7.0; Langmuir SA = 1733 $m^2\ g^{-1}$).

### 3.2. Synthesis and Characterization of reo-MOF-$1_A$.

Assuming that the sulfonate functionalities can prevent successful sample activation, a linker-exchange reaction of **reo**-MOF-1 with pristine $NDC^{2-}$ linkers may solve the sample activation challenge. To this end, **reo**-MOF-1 was subjected to linker exchange with dipotassium naphthalene-2,6-dicarboxylate ($K_2NDC$), where the potassium salt was used to facilitate the linker-exchange rate (Figure 1c,d). After performing the linker-exchange procedure for 30 min, the resulting MOF powder was washed and dried (see Experimental Section).

PXRD and spectroscopic analyses of the activated **reo**-MOF-$1_A$ sample were performed to evaluate whether $SNDC^{3-}$ linkers in **reo**-MOF-1 are replaced with $NDC^{2-}$ without loss in framework crystallinity. The PXRD pattern (Figure 3b) indicates that the linker-exchanged sample remains highly crystalline, which is in sharp contrast to the diffraction pattern of **reo**-MOF-1. Successful linker exchange is also confirmed by the FT-IR spectra; two unique peaks centered at 1180 and 1649 $cm^{-1}$, which were assigned to the sulfonate and carboxylate stretching modes of the $HSNDC^{2-}$/$SNDC^{3-}$ linker, respectively (Figure 3a), were absent in the FT-IR spectrum of **reo**-MOF-$1_A$. To determine the ratio of $HSNDC^{2-}$ (acidified at pH = 1) and $NDC^{2-}$ in **reo**-MOF-$1_A$ quantitatively, $^1H$ NMR spectrum of acid-digested samples


DOI: 10.1021/acsami.8b11037
ACS Appl. Mater. Interfaces 2018, 10, 35462−35468

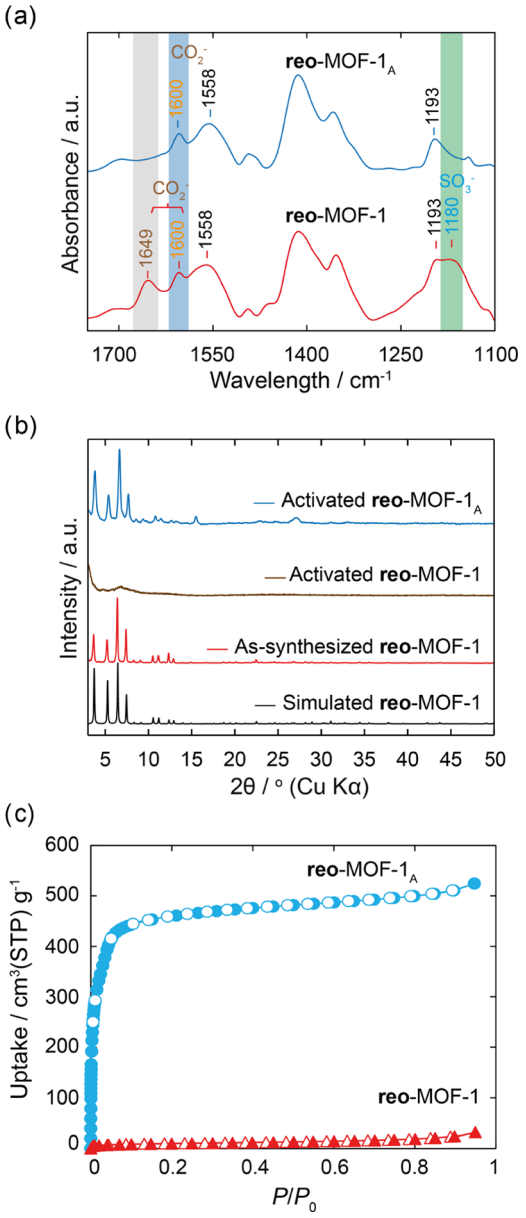


**Figure 3.** Characterizations of **reo**-MOF-1 and **reo**-MOF-$1_A$: Fourier transform-infrared spectroscopy analysis (a); powder X-ray diffraction analysis (b) and $N_2$ adsorption isotherms (c).

was recorded. From the integration of $H_d$ (H atom at C1 position of $HSNDC^{2-}$), the $HSNDC^{2-}/NDC^{2-}$ ratio is estimated to be 0.14 (Figure S15). With EA data, a plausible chemical formula of **reo**-MOF-$1_A$ can be determined as $[Zr_6O_8(H_2O)_6(NDC)_{4.38}(HSNDC)_{0.62}]\cdot 3.27(H_2O)$.[54]

The thermal stability and the permanent porosity of **reo**-MOF-$1_A$ were examined by thermogravimetric analysis (TGA) and 77 K $N_2$ adsorption measurements. TGA indicates that **reo**-MOF-$1_A$ is stable up to 450 °C with less than 2.2% weight loss up to 200 °C (Figure S11). $N_2$ isotherm of **reo**-MOF-$1_A$ shows reversible uptake (Figure 3c) with a high BET (Langmuir) surface area of 2104 $m^2\ g^{-1}$ (2203 $m^2\ g^{-1}$). These values are in line with the theoretically predicted surface area (Materials Studio 7.0; Langmuir SA = 2083 $m^2\ g^{-1}$) and are higher than those of **reo**-MOF-1 (42 $m^2\ g^{-1}$, structural collapse), pristine UiO-66 (1187 $m^2\ g^{-1}$),[46] UiO-66 with missing linker defects (1617 $m^2\ g^{-1}$),[22] UiO-66 missing cluster defects (1777 $m^2\ g^{-1}$),[34] and DUT-52 (1399 $m^2\ g^{-1}$).[45] Furthermore, pore size distribution analysis confirmed the pore diameters in **reo**-MOF-$1_A$ (Figure S29).

**3.3. Catalytic Activity.** Recently, the design and synthesis of new Zr-based MOFs with large pore sizes and strong Brønsted acid catalytic activity have received much attention.[47,55−57] As we demonstrated, **reo**-MOF-$1_A$ exhibits a high surface area, and more importantly the pores of **reo**-MOF-$1_A$ are decorated with residual sulfonic acid groups. This led us to evaluate the Brønsted acid catalytic activity of **reo**-MOF-$1_A$ in comparison to representative Zr-based MOFs. For this purpose, we chose the formation of 2-phenylbenzoxazole by the condensation reaction between benzaldehyde and 2-aminophenol because of its emissive properties and pharmaceutical interests.[58,59] The catalytic activity of **reo**-MOF-$1_A$ was evaluated according to a published procedure with a slight modification.[55] After combining benzaldehyde and 2-aminophenol in the presence of **reo**-MOF-$1_A$, the color of the reaction mixture gradually turned from black purple to red brown, which is indicative of the successful formation of 2-phenylbenzoxazole. Gas chromatography (GC) analysis revealed that 2-phenylbenzoxazole was formed with 99% GC yield (92% isolated yield) in the presence of 1 mol % **reo**-MOF-$1_A$ catalyst after 6 h. To exclude the possibility that the condensation reaction is catalyzed by the acidic linker molecules leached out from **reo**-MOF-$1_A$, we performed control experiments. As expected, no 2-phenylbenzoxazole formation was observed after the isolation of **reo**-MOF-$1_A$ from the reaction mixture (Figure 4), indicating that **reo**-MOF-$1_A$ works as a heterogeneous catalyst.

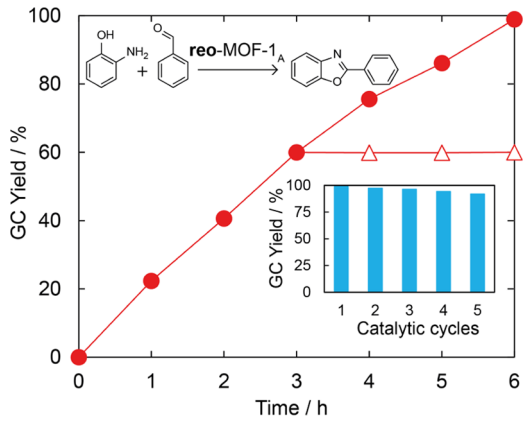


**Figure 4.** GC yield percentage of 2-phenylbenzoxazole as a function of reaction time in the presence of **reo**-MOF-$1_A$ (red cycle) and the control reaction following removal of **reo**-MOF-$1_A$ from the reaction after 3 h catalysis (red triangle). Inset: catalyst recycling studies of **reo**-MOF-$1_A$.

The durability of **reo**-MOF-$1_A$ as a catalyst was further evaluated by repeating the catalysis experiments for up to five cycles. Experimental results exhibited that **reo**-MOF-$1_A$ is reused without a significant reduction in catalytic activity. Specifically, up to 92% GC yield was found after the fifth cycle with the recovered **reo**-MOF-$1_A$ powder sample (Figure 4). Moreover, no significant structural degradation of **reo**-MOF-$1_A$ was observed following these consecutive catalytic experiments, based on PXRD and FT-IR measurements (Section S11). To further demonstrate the advantage of **reo**-MOF-$1_A$ as a Brønsted acid catalyst, the catalytic activity was compared


DOI: 10.1021/acsami.8b11037
ACS Appl. Mater. Interfaces 2018, 10, 35462−35468

**Table 1. Reactions between Aldehyde and 2-Aminophenol Utilizing Different Catalysts[a]**

| entry | catalyst | yield (%) |
|---|---|---|
| 1 | **reo**-MOF-$1_A$ | 98.6 ± 0.23 (92[b]) |
| 2 | acidified **reo**-MOF-1 | 59.5 ± 0.37 |
| 3 | DUT-52 | 53.3 ± 0.38 |
| 4 | UiO-67 | 40.5 ± 0.44 |
| 5 | UiO-66 | 24.6 ± 0.36 |
| 6 | MOF-808-P | 46.7 ± 0.39 |
| 7 | NU-1000 | 75.3 ± 0.55 |

[a]Reaction conditions: 1 mol % catalyst, benzaldehyde (0.5 mmol), 2-aminophenol (0.5 mmol), 6 h. [b]Isolated yield.

with **reo**-MOF-1 (acidified at pH = 1 for 24 h), DUT-52, UiO-66, UiO-67, MOF-808-P, and NU-1000. As shown in Table 1 and Figure S24, catalytic activity of **reo**-MOF-$1_A$ is significantly higher than those of other Zr-based MOFs. This can be attributed to a combination of effects; faster diffusion of substrates through the larger pores along with acidic functionalities decorating the pore walls accelerates the condensation reaction.

To take this point further, we performed the linker-exchange reaction for varying lengths of time (10 min and 14 h) to modulate the density of acidic functional groups that line the framework interior (Table 2). PXRD patterns of these activated samples confirm that high crystallinity is retained following linker exchange (Figure S27). The BET surface areas of MOF samples exchanged for 10 min and 14 h were calculated to be 1704 and 2218 $m^2\ g^{-1}$, respectively (Figure S28). Furthermore, the pore size distribution analysis indicates that the pore width for the 14 h exchanged sample is slightly larger than the samples exchanged for a shorter time because of the replacement of a greater amount of bulky functional groups (Figure S29). Indeed, this trend is in line with FT-IR and $^1$H NMR spectra as the $HSNDC^{2-}$ content decreases with an increase in the linker-exchange time (Figures S30 and S31).

The catalytic investigations of these samples were performed in the same manner. The GC yields of 10 min and 14 h samples were estimated to be 42.0 and 54.4%, respectively, which is significantly lower than **reo**-MOF-$1_A$ (30 min sample, 98.6% of GC yield, Figure S32). The low catalytic activity of the sample treated for 10 min can be attributed to the high concentration of bulky $HSNDC^{2-}$ linker, preventing substrate diffusion. In contrast, it is presumed that the lower density of acidic sites in the sample treated for 14 h leads to limited catalytic activity. These results support our hypothesis that the **reo** architecture that is decorated with an optimal density of acidic functionalities offers the best of both worlds, allowing the diffusion of substrates while maintaining a significant number of Brønsted acid sites for maximal activity.

## 4. CONCLUSIONS

In this work, we describe the synthesis and characterization of a new Zr-based MOF, **reo**-MOF-1, prepared by combining linker design and linker-exchange strategies. The outcome of this study demonstrates that the coordination number of Zr-based clusters can be controlled by employing linkers functionalized with sulfonate moieties whose steric hindrance prevents the formation of a framework with the maximal coordination number of 12; instead, a more open framework offering larger cavities forms, with 8-coordinated inorganic clusters while maintaining the sought-after chemical stability that has made Zr-based MOFs famous. This difference in the coordination number plays a key role in the formation of the **reo** architecture. The new material, **reo**-MOF-1, was further treated in an aqueous solution containing $K_2NDC$ to replace part of the $SNDC^{3-}$ linkers. After the linker-exchange reaction, the resulting material **reo**-MOF-$1_A$ exhibited permanent porosity with a high BET surface area (2104 $m^2\ g^{-1}$). The combination of this open-framework structure with the presence of residual sulfonic acid functionalities in the pores leads to superior catalytic performance, exemplified by the condensation reaction to form 2-phenylbenzoxazole using **reo**-MOF-$1_A$ as the catalyst. Indeed, the latter outperformed representative Zr-based MOF materials. We anticipate that our strategy will inspire the design of new porous frameworks, such as reticularly expanded forms of **reo**-MOF-1 and frameworks with multivariate functionalities,[60] maximizing the performance of this class of materials as Brønsted acid catalysts.

## ■ ASSOCIATED CONTENT

### Supporting Information

The Supporting Information is available free of charge on the ACS Publications website at DOI: 10.1021/acsami.8b11037.

Full synthesis and characterization; crystallographic data; catalysis study of **reo**-MOF-1 and **reo**-MOF-$1_A$ (PDF)

## ■ AUTHOR INFORMATION


### Corresponding Author

*E-mail: tnthach@ntt.edu.vn, tnthach@inomar.edu.vn.

### ORCID

Thach N. Tu: 0000-0003-4240-0224
Tien H. N. Lo: 0000-0003-2108-6344
Hiroyasu Furukawa: 0000-0002-6082-1738
My D. Nguyen: 0000-0002-8866-6602

### Present Address

⊥Intelligent & Sustainable Materials Group, Korea Institute of Industrial Technology, 89 Yangdaegiro-gil, Ipjang-myeon, Cheonan-si 31056, South Korea (T.H.N.L.).


### Author Contributions

T.N.T. formulated the project. T.H.N.L., M.V.N., H.T.T.N., N.N.N., and M.D.N. synthesized the compounds. H.T.T.N. collected isotherms, powder X-ray diffraction patterns, and FT-IR spectra and performed catalytic studies. T.N.T. solved crystal structure and analyzed all experimental data. T.N.T. and H.F. wrote the paper and all authors contributed to revising it. All authors have given approval to the final version of the manuscript.

**Table 2. Probing the Relationship between Catalytic Activity and the Concentration of Acidic Functionalities**

| linker-exchange time | catalyst | $HSNDC^{2-}/NDC^{2-}$ | BET surface area ($m^2\ g^{-1}$) | GC yield (%) |
|---|---|---|---|---|
| 10 min | 10 min **reo**-MOF-$1_A$ | 0.32 | 1704 | 41.6 ± 0.31 |
| 30 min | 30 min **reo**-MOF-$1_A$ (original sample) | 0.14 | 2104 | 98.6 ± 0.23 |
| 14 h | 14 h **reo**-MOF-$1_A$ | 0.07 | 2218 | 53.7 ± 0.48 |



DOI: 10.1021/acsami.8b11037
ACS Appl. Mater. Interfaces 2018, 10, 35462−35468

## Notes

The authors declare no competing financial interest.

## ■ ACKNOWLEDGMENTS

We are grateful to Prof. Omar M. Yaghi (UC Berkeley) for the continued support for global science initiatives. This research was supported by the U.S. Office of Naval Research Global: Naval International Cooperative Opportunities in Science and Technology Program (No. N62909-16-1-2146) for the linker synthesis, materials characterization, and catalysis. The authors also acknowledge the financial support from Nguyen Tat Thanh University for the design, synthesis, and structural determination of **reo**-MOF-1 and **reo**-MOF-$1_A$. We acknowledge Dr. Christopher A. Trickett for his valuable comments and editorial assistance. We thank Y. B. N. Tran, Huong Nguyen, and Vu D. Tieu at INOMAR for their assistance with this work.

## ■ REFERENCES

(1) Furukawa, H.; Cordova, K. E.; O'Keeffe, M.; Yaghi, O. M. The Chemistry and Applications of Metal−Organic Frameworks. *Science* **2013**, *341*, No. 1230444, DOI: 10.1126/science.1230444.

(2) Adil, K.; Belmabkhout, Y.; Pillai, R. S.; Cadiau, A.; Bhatt, P. M.; Assen, A. H.; Maurin, G.; Eddaoudi, M. Gas/Vapour Separation Using Ultra-Microporous Metal−Organic Frameworks: Insights into the Structure/Separation Relationship. *Chem. Soc. Rev.* **2017**, *46*, 3402−3430.

(3) Peng, Y.; Krungleviciute, V.; Eryazici, I.; Hupp, J. T.; Farha, O. K.; Yildirim, T. Methane Storage in Metal−Organic Frameworks: Current Records, Surprise Findings, and Challenges. *J. Am. Chem. Soc.* **2013**, *135*, 11887−11894.

(4) Meng, X.; Wang, H. N.; Song, S. Y.; Zhang, H. J. Proton-Conducting Crystalline Porous Materials. *Chem. Soc. Rev.* **2017**, *46*, 464−480.

(5) Tu, T. N.; Phan, N. Q.; Vu, T. T.; Nguyen, H. L.; Cordova, K. E.; Furukawa, H. High Proton Conductivity at Low Relative Humidity in an Anionic Fe-Based Metal−Organic Framework. *J. Mater. Chem. A* **2016**, *4*, 3638−3641.

(6) Yang, F.; Xu, G.; Dou, Y.; Wang, B.; Zhang, H.; Wu, H.; Zhou, W.; Li, J. R.; Chen, B. A Flexible Metal−Organic Framework with a High Density of Sulfonic Acid Sites for Proton Conduction. *Nat. Energy* **2017**, *2*, 877−883.

(7) Huang, Y. B.; Liang, J.; Wang, X. S.; Cao, R. Multifunctional Metal−Organic Framework Catalysts: Synergistic Catalysis and Tandem Reactions. *Chem. Soc. Rev.* **2017**, *46*, 126−157.

(8) Pham, P. H.; Doan, S. H.; Tran, H. T. T.; Nguyen, N. N.; Phan, A. N. Q.; Le, H. V.; Tu, T. N.; Phan, N. T. S. A New Transformation of Coumarins via Direct C−H Bond Activation Utilizing an Iron−Organic Framework as a Recyclable Catalyst. *Catal. Sci. Technol.* **2018**, *8*, 1267−1271.

(9) Wuttke, S.; Lismont, M.; Escudero, A.; Rungtaweevoranit, B.; Parak, W. J. Positioning Metal-organic Framework Nanoparticles within the Context of Drug Delivery − A Comparison with Mesoporous Silica Nanoparticles and Dendrimers. *Biomaterials* **2017**, *123*, 172−183.

(10) Freund, R.; Lächelt, U.; Gruber, T.; Rühle, B.; Wuttke, S. Multifunctional Efficiency: Extending the Concept of Atom Economy to Functional Nanomaterials. *ACS Nano* **2018**, *12*, 2094−2105.

(11) Deria, P.; Gualdron, D. A. G.; Bury, W.; Schaef, H. T.; Wang, T. C.; Thallapally, P. K.; Sarjeant, A. A.; Snurr, R. Q.; Hupp, J. T.; Farha, O. K. Ultraporous, Water Stable, and Breathing Zirconium-based Metal−Organic Frameworks with **ftw** Topology. *J. Am. Chem. Soc.* **2015**, *137*, 13183−13190.

(12) DeCoste, J. B.; Peterson, G. W.; Jasuja, H.; Glover, T. G.; Huang, Y.; Walton, K. S. Stability and Degradation Mechanisms of Metal-Organic Frameworks Containing the $Zr_6O_4(OH)_4$ Secondary Building Unit. *J. Mater. Chem. A* **2013**, *1*, 5642−5650.

(13) Howarth, A. J.; Liu, Y.; Li, P.; Li, Z.; Wang, T. C.; Hupp, J. T.; Farha, O. K. Chemical, Thermal and Mechanical Stabilities of Metal−Organic Frameworks. *Nat. Rev. Mater.* **2016**, *1*, No. 15018.

(14) Shearer, G. C.; Chavan, S.; Ethiraj, J.; Vitillo, J. G.; Svelle, S.; Olsbye, U.; Lamberti, C.; Bordiga, S.; Lillerud, K. P. Tuned to Perfection: Ironing Out the Defects in Metal−Organic Framework UiO-66. *Chem. Mater.* **2014**, *26*, 4068−4071.

(15) Bai, Y.; Dou, Y.; Xie, L. H.; Rutledge, W.; Li, J. R.; Zhou, H.-C. Zr-Based Metal−Organic Frameworks: Design, Synthesis, Structure, and Applications. *Chem. Soc. Rev.* **2016**, *45*, 2327−2367.

(16) Lippke, J.; Brosent, B.; von Zons, T.; Virmani, E.; Lilienthal, S.; Preuße, T.; Hu, M.; Schneider, A. M.; Wuttke, S.; Behrens, P.; Godt, A. Expanding the Group of Porous Interpenetrated Zr-Organic Frameworks (PIZOFs) with Linkers of Different Lengths. *Inorg. Chem.* **2017**, *56*, 748−761.

(17) Fang, Z.; Bueken, B.; De Vos, D. E.; Fischer, R. A. Defect-Engineered Metal−Organic Frameworks. *Angew. Chem., Int. Ed.* **2015**, *54*, 7234−7254.

(18) Ren, J.; Ledwaba, M.; Musyoka, N. M.; Langmi, H. W.; Mathe, M.; Liao, S.; Pang, W. Structural Defects in Metal−Organic Frameworks (MOFs): Formation, Detection and Control towards Practices of Interests. *Coord. Chem. Rev.* **2017**, *349*, 169−197.

(19) Tu, T. N.; Nguyen, M. V.; Nguyen, H. L.; Yuliarto, B.; Cordova, K. E.; Demir, S. Designing Bipyridine-Functionalized Zirconium Metal−Organic Frameworks as a Platform for Clean Energy And Other Emerging Applications. *Coord. Chem. Rev.* **2018**, *364*, 33−50.

(20) Yuan, S.; Qin, J. S.; Zou, L.; Chen, Y. P.; Wang, X.; Zhang, Q.; Zhou, H.-C. Thermodynamically Guided Synthesis of Mixed-Linker Zr-MOFs with Enhanced Tunability. *J. Am. Chem. Soc.* **2016**, *138*, 6636−6642.

(21) Huang, H.; Li, J.; Wang, K.; Han, T.; Tong, M.; Li, L.; Xie, Y.; Yang, Q.; Liu, D.; Zhong, C.; et al. An in Situ Self-Assembly Template Strategy for the Preparation of Hierarchical-Pore Metal−Organic Frameworks. *Nat. Commun.* **2015**, *6*, No. 8847, DOI: 10.1038/ncomms9847.

(22) Wu, H.; Chua, Y. S.; Krungleviciute, V.; Tyagi, M.; Chen, P.; Yildirim, T.; Zhou, W. Unusual and Highly Tunable Missing-Linker Defects in Zirconium Metal−Organic Framework UiO-66 and Their Important Effects on Gas Adsorption. *J. Am. Chem. Soc.* **2013**, *135*, 10525−10532.

(23) Liang, W.; Coghlan, C. J.; Ragon, F.; Martinez, M. R.; D'Alessandro, D. M.; Babarao, R. Defect Engineering of UiO-66 for $CO_2$ and $H_2O$ Uptake−A Combined Experimental and Simulation Study. *Dalton Trans.* **2016**, *45*, 4496−4500.

(24) Taylor, J. M.; Komatsu, T.; Dekura, S.; Otsubo, K.; Takata, M.; Kitagawa, H. The Role of A Three Dimensionally Ordered Defect Sublattice on the Acidity of a Sulfonated Metal−Organic Framework. *J. Am. Chem. Soc.* **2015**, *137*, 11498−11506.

(25) Taylor, J. M.; Dekura, S.; Ikeda, R.; Kitagawa, H. Defect Control to Enhance Proton Conductivity in a Metal−Organic Framework. *Chem. Mater.* **2015**, *27*, 2286−2289.

(26) Liu, Y.; Klet, R. C.; Hupp, J. T.; Farha, O. Probing the Correlations Between the Defects in Metal−Organic Frameworks and Their Catalytic Activity by an Epoxide Ring-Opening Reaction. *Chem. Commun.* **2016**, *52*, 7806−7809.

(27) Ye, G.; Zhang, D.; Li, X.; Leng, K.; Zhang, W.; Ma, J.; Sun, Y.; Xu, W.; Ma, S. Boosting Catalytic Performance of Metal−Organic Framework by Increasing the Defects via a Facile and Green Approach. *ACS Appl. Mater. Interfaces* **2017**, *9*, 34937−34943.

(28) Liang, W.; Li, L.; Hou, J.; Shepherd, N. D.; Bennett, T. D.; D'Alessandro, D. M.; Chen, V. Linking Defects, Hierarchical Porosity Generation and Desalination Performance in Metal−Organic Frameworks. *Chem. Sci.* **2018**, *9*, 3508−3516.

(29) Gutov, O. V.; Hevia, M. G.; Adán, E. C. E.; Shafir, A. Metal−Organic Framework (MOF) Defects under Control: Insights into the Missing Linker Sites and Their Implication in the Reactivity of Zirconium-Based Frameworks. *Inorg. Chem.* **2015**, *54*, 8396−8400.



DOI: 10.1021/acsami.8b11037
*ACS Appl. Mater. Interfaces* 2018, 10, 35462−35468

(30) Peterson, G. W.; Destefano, M. R.; Garibay, S. J.; Ploskonka, A.; McEntee, M.; Hall, M.; Karwacki, C. J.; Hupp, J. T.; Farha, O. K. Optimizing Toxic Chemical Removal Through Defect-Induced UiO-66-$NH_2$ Metal−Organic Framework. *Chem. - Eur. J.* **2017**, *23*, 15913−15916.
(31) Carboni, M.; Lin, Z.; Abney, C. W.; Zhang, T.; Lin, W. A Metal−Organic Framework Containing Unusual Eight-Connected Zr−Oxo Secondary Building Units and Orthogonal Carboxylic Acids for Ultra-Sensitive Metal Detection. *Chem. - Eur. J.* **2014**, *20*, 14965−14970.
(32) Chaemchuen, S.; Luo, Z.; Zhou, K.; Mousavi, B.; Phatanasri, S.; Jaroniec, M.; Verpoort, F. Defect Formation in Metal−Organic Frameworks Initiated by the Crystal Growth-Rate and Effect on Catalytic Performance. *J. Catal.* **2017**, *354*, 84−91.
(33) DeStefano, M. R.; Islamoglu, T.; Garibay, S. J.; Hupp, J. T.; Farha, O. K. Room-Temperature Synthesis of UiO-66 and Thermal Modulation of Densities of Defect Sites. *Chem. Mater.* **2017**, *29*, 1357−1361.
(34) Shearer, G. C.; Chavan, S.; Bordiga, S.; Svelle, S.; Olsbye, U.; Lillerud, K. P. Defect Engineering: Tuning the Porosity and Composition of the Metal−Organic Framework UiO-66 via Modulated Synthesis. *Chem. Mater.* **2016**, *28*, 3749−3761.
(35) Trickett, C. A.; Gagnon, K. J.; Lee, S.; Gándara, F.; Bürgi, H. B.; Yaghi, O. M. Definitive Molecular Level Characterization of Defects in UiO-66 Crystals. *Angew. Chem., Int. Ed.* **2015**, *54*, 11162−11167.
(36) Cai, G.; Jiang, H. L. A Modulator-Induced Defect-Formation Strategy to Hierarchically Porous Metal−Organic Frameworks with High Stability. *Angew. Chem., Int. Ed.* **2017**, *56*, 563−567.
(37) Feng, L.; Yuan, S.; Zhang, L. L.; Tan, K.; Li, J. L.; Kirchon, A.; Liu, L. M.; Zhang, P.; Han, Y.; Chabal, Y. J.; Zhou, H.-C. Creating Hierarchical Pores by Controlled Linker Thermolysis in Multivariate Metal−Organic Frameworks. *J. Am. Chem. Soc.* **2018**, *140*, 2363−2372.
(38) Bueken, B.; Velthoven, N. V.; Krajnc, A.; Smolders, S.; Taulelle, F.; Draznieks, C. M.; Mali, G.; Bennett, T. D.; Vos, D. D. Tackling the Defect Conundrum in UiO-66: A Mixed-Linker Approach to Engineering Missing Linker Defects. *Chem. Mater.* **2017**, *29*, 10478−10486.
(39) Gadipelli, S.; Guo, Z. Postsynthesis Annealing of MOF-5 Remarkably Enhances the Framework Structural Stability and $CO_2$ Uptake. *Chem. Mater.* **2014**, *26*, 6333−6338.
(40) Yuan, S.; Zou, L.; Qin, J. S.; Li, J.; Huang, L.; Feng, L.; Wang, X.; Bosch, M.; Alsalme, A.; Cagin, T.; Zhou, H.-C. Construction of Hierarchically Porous Metal−Organic Frameworks Through Linker Labilization. *Nat. Commun.* **2017**, *8*, No. 15356.
(41) Hu, Z.; Peng, Y.; Gao, Y.; Qian, Y.; Ying, S.; Yuan, D.; Horike, S.; Ogiwara, N.; Babarao, R.; Wang, Y.; Yan, N.; Zhao, D. Direct Synthesis of Hierarchically Porous Metal−Organic Frameworks with High Stability and Strong Brønsted Acidity: The Decisive Role of Hafnium in Efficient and Selective Fructose Dehydration. *Chem. Mater.* **2016**, *28*, 2659−2667.
(42) Schrimpf, W.; Jiang, J.; Ji, Z.; Hirschle, P.; Lamb, D. C.; Yaghi, O. M.; Wuttke, S. Chemical Diversity in a Metal−Organic Framework Revealed by Fluorescence Lifetime Imaging. *Nat. Commun.* **2018**, *9*, No. 1647.
(43) Foo, M. L.; Horike, S.; Fukushima, T.; Hijikata, Y.; Kubota, Y.; Takata, M.; Kitagawa, S. Ligand-Based Solid Solution Approach to Stabilisation of Sulphonic Acid Groups in Porous Coordination Polymer $Zr_6O_4(OH)_4(BDC)_6$ (UiO-66). *Dalton Trans.* **2012**, *41*, 13791−13794.
(44) Cliffe, M. J.; Wan, W.; Zou, X.; Chater, P. A.; Kleppe, A. K.; Tucker, M. G.; Wilhelm, H.; Funnell, N. P.; Coudert, F. X.; Goodwin, A. L. Correlated Defect Nanoregions in a Metal−Organic Framework. *Nat. Commun.* **2014**, *5*, No. 4176.
(45) Bon, V.; Senkovska, I.; Weiss, M. S.; Kaskel, S. Tailoring of Network Dimensionality and Porosity Adjustment in Zr- and Hf-Based MOFs. *CrystEngComm* **2013**, *15*, 9572−9577.
(46) Cavka, J. H.; Jakobsen, S.; Olsbye, U.; Guillou, N.; Lamberti, C.; Bordiga, S.; Lillerud, K. P. A New Zirconium Inorganic Building Brick Forming Metal Organic Frameworks with Exceptional Stability. *J. Am. Chem. Soc.* **2008**, *130*, 13850−13851.
(47) Jiang, J.; Gándara, F.; Zhang, Y. B.; Na, K.; Yaghi, O. M.; Klemperer, W. G. Superacidity in Sulfated Metal−Organic Framework-808. *J. Am. Chem. Soc.* **2014**, *136*, 12844−12847.
(48) Mondloch, J. E.; Bury, W.; Jimenez, D. F.; Kwon, S.; Demarco, E. J.; Weston, M. H.; Sarjeant, A. A.; Nguyen, S. T.; Stair, P. C.; Snurr, R. Q.; Farha, O. K.; Hupp, J. T. Vapor-Phase Metalation by Atomic Layer Deposition in a Metal−Organic Framework. *J. Am. Chem. Soc.* **2013**, *135*, 10294−10297.
(49) Lo, T. H. N.; Nguyen, M. V.; Tu, T. N. An Anchoring Strategy Leads to Enhanced Proton Conductivity in a New Metal−Organic Framework. *Inorg. Chem. Front.* **2017**, *4*, 1509−1516.
(50) Nguyen, M. V.; Lo, T. H. N.; Luu, L. C.; Nguyen, H. T. T.; Tu, T. N. Enhancing Proton Conductivity in a Metal−Organic Framework at T > 80 °C by an Anchoring Strategy. *J. Mater. Chem. A* **2018**, *6*, 1816−1821.
(51) The partial deprotonation of sulfonic acid functionalities are found in **reo**-MOF-1.
(52) Bon, V.; Senkovskyy, V.; Senkovska, I.; Kaskel, S. Zr(IV) and Hf(IV) Based Metal−Organic Frameworks with **reo**-Topology. *Chem. Commun.* **2012**, *48*, 8407−8409.
(53) Drache, F.; Bon, V.; Senkovska, I.; Marschelke, C.; Synytska, A.; Kaskel, S. Postsynthetic Inner-Surface Functionalization of the Highly Stable Zirconium-Based Metal−Organic Framework DUT-67. *Inorg. Chem.* **2016**, *55*, 7206−7213.
(54) EA shows that the carbon content is higher than expected. This could be because naphthalene-2,6-dicarboxylate is exchanged with the coordinated formate ligands (introduced during the solvothermal synthesis).
(55) Nguyen, L. H. T.; Nguyen, T. T.; Nguyen, H. L.; Doan, T. L. H.; Tran, P. H. A New Superacid Hafnium-Based Metal−Organic Framework as a Highly Active Heterogeneous Catalyst for the Synthesis of Benzoxazoles under Solvent-Free Conditions. *Catal. Sci. Technol.* **2017**, *7*, 4346−4350.
(56) Ly, H. G. T.; Fu, G.; Kondinski, A.; Bueken, B.; Vos, D. D.; Vogt, T. N. P. Superactivity of MOF-808 toward Peptide Bond Hydrolysis. *J. Am. Chem. Soc.* **2018**, *140*, 6325−6335.
(57) Dou, Y.; Zhang, H.; Zhou, A.; Yang, F.; Shu, L.; She, Y.; Li, J. R. Highly Efficient Catalytic Esterification in an $-SO_3H$-Functionalized Cr(III)-MOF. *Ind. Eng. Chem. Res.* **2018**, *57*, 8388−8395.
(58) Carayon, C.; Forgues, S. F. 2-Phenylbenzoxazole Derivatives: a Family of Robust Emitters of Solid-State Fluorescence. *Photochem. Photobiol. Sci.* **2017**, *16*, 1020−1035.
(59) Zhang, W.; Liu, J.; Macho, J. M.; Jiang, X.; Xie, D.; Jiang, F.; Liu, W.; Fu, L. Design, Synthesis and Antimicrobial Evaluation of Novel Benzoxazole Derivatives. *Eur. J. Med. Chem.* **2017**, *126*, 7−14.
(60) Furukawa, H.; Müller, U.; Yaghi, O. M. "Heterogeneity within Order" in Metal−Organic Frameworks. *Angew Chem., Int. Ed.* **2015**, *54*, 3417−3430.


DOI: 10.1021/acsami.8b11037
*ACS Appl. Mater. Interfaces* 2018, 10, 35462−35468